Electronic Supplementary Material (ESI) for Sustainable Energy & Fuels.

Supplementary Material

Light transfer through bubble-filled electrolyte for solar water splitting

Abhinav Bhanawat and Laurent Pilon[+]

Mechanical and Aerospace Engineering Department

Henry Samueli School of Engineering and Applied Science

University of California, Los Angeles

[+]Corresponding Author: Phone: +1 (310)-206-5598, Fax: +1 (310)-206-2302

Engineering IV

420 Westwood Plaza, Los Angeles, CA 90095-1597

E-mail: pilon@seas.ucla.edu

S1. Computational Monte Carlo ray-tracing procedure

i. Generate a random initial position in the x-y plane on top of the computational domain for the normally incident ray.

ii. Determine the next location reached by the ray at either the electrolyte/bubble interface, the electrolyte/photoelectrode interface, or the bubble/photoelectrode interface. If that location was inside the photoelectrode e.g., for rays refracted into surface-attached bubbles (see Figure 2), update it to a location on the photoelectrode surface by retracing the ray while maintaining the same direction.

iii. Calculate the distance l travelled by the ray through the medium from the previous location to the final position.

iv. Generate a random number rd between 0 and 1 following a uniform distribution to calculate a random path length l'_m given by $l'_m = ln(rd/\kappa_{m,\lambda})$ where $\kappa_{m,\lambda} = 4\pi k_{m,\lambda}/\lambda$ is the absorption coefficient of the medium. If $l > l'_m$, count the ray as absorbed in the medium. If $l < l'_m$, calculate the interface reflectance ρ using Fresnel's equations.

v. Again, generate a random number rd between 0 and 1 following a uniform distribution. If $rd < \rho$, then the ray was reflected, else it was refracted. For either case, update the ray direction accordingly using the generalized Snell's law [1].

vi. With this new position and updated direction, trace the ray again in its onward journey to another interface by repeating steps 2-5.

vii. If the ray reached the top surface of the computational domain, count it as reflected.

If it was refracted into the photoelectrode through either the bubble/photoelectrode or the electrolyte/photoelectrode interface, count it as absorbed in the photoelectrode.

S2. Validation of MCRT code

Figure S1 schematically shows the three simulation cases for which the the analytical expressions for the area-averaged photoelectrode absorptance $\bar{A}_\lambda$ were available from Refs. [2, 3]. The three simulation cases are detailed below.

Case I

Here, the refractive and absorption indices of the bubbles were chosen to be the same as that of the electrolyte, equivalent to having a semitransparent electrolyte of thickness $H_e = 10$ mm covering the photoelectrode without any bubbles, as shown schematically in Figure S1(a). Thus, the photoelectrode absorptance was given by [2]

$$\bar{A}_{I,\lambda} = (1 - \rho_{ep,\lambda}) e^{-\kappa_{e,\lambda} H_e}, \tag{S.1}$$

where the subscripts I refers to Case I, $\kappa_{e,\lambda} = 4\pi k_{e,\lambda}/\lambda$ and $\rho_{ij,\lambda}$ is the reflectance at the optically smooth interface between media i and j under normal incidence, given by [2]

$$\rho_{ij,\lambda} = \frac{(n_{i,\lambda} - n_{j,\lambda})^2 + (k_{i,\lambda} - k_{j,\lambda})^2}{(n_{i,\lambda} + n_{j,\lambda})^2 + (k_{i,\lambda} + k_{j,\lambda})^2} \tag{S.2}$$

Case II

Here, a gas film of thickness $H_b = 1$ mm having refrative index same as the bubbles was embedded between the Si photoelectrode and a non-absorbing electrolyte of thickenss $H_e = 9$ mm, as shown schematically in Figure S1(b). Here, the photoelectrode absorptance was

given by [2]

$$\bar{A}_{II,\lambda} = \frac{(1-\rho_{eb,\lambda})(1-\rho_{bp,\lambda})}{1-\rho_{eb,\lambda}\rho_{bp,\lambda}}, \tag{S.3}$$

where the subscripts e, b, and p respectively represent the electrolyte, the bubble and the photoelectrode and $\rho_{ij,\lambda}$ is given by Eq. S.3.

Case III

Here, a gas film of thickness $H_b = 1$ mm having refrative index same as the bubbles was embedded between two non-absorbing layers of electrolyte, each having thickenss $H = 4.5$ mm, as shown schematically in Figure S1(c). Here, the photoelectrode absorptance was given by [3]

$$\bar{A}_{III,\lambda} = \frac{(1-\rho_{eb,\lambda})(1-\rho_{be,\lambda})(1-\rho_{ep,\lambda})}{(1-\rho_{eb,\lambda}\rho_{be,\lambda})(1-\rho_{be,\lambda}\rho_{ep,\lambda}) - (1-\rho_{be,\lambda})\rho_{eb,\lambda}\rho_{ep,\lambda}}. \tag{S.4}$$

Here again, the subscripts e, b, and p respectively represent the electrolyte, the bubble and the photoelectrode and $\rho_{ij,\lambda}$ is given by Eq. S.3.

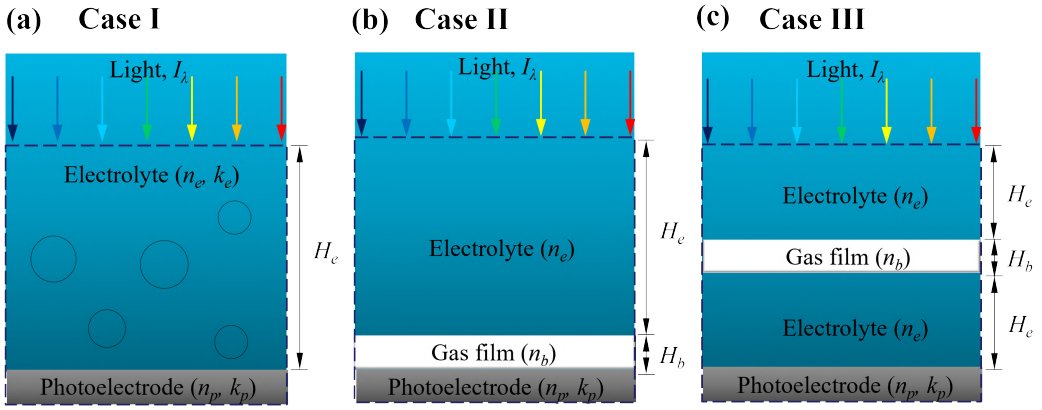

Figure S1: Schematics for (a) Case I, (b) Case II, and (c) Case III chosen for validating the MCRT code.

Figure S2(a) plots the area-averaged photoelectrode absorptance $\bar{A}_\lambda$ as a function of wavelength λ of the incident radiation for the three cases considered. It shows excellent agreement between the analytical and numerical predictions for all wavelengths, thus validating that reflection and refraction at the electrolyte/bubble, bubble/photoelectrode, and electrolyte/bubble interfaces, as well as absorption by the electrolyte were accurately accounted for.

Moreover, the area-averaged absorptance of a bubble-covered horizontal Si photoelectrode subjected to normally incident monochromatic radiation of wavelength $\lambda = 630$ nm was predicted and compared with those reported in Ref.[4] assuming no bubbles dispersed in the transparent electrolyte volume. For these simulations, the bubble plume thickness H and the bubble diameter D were chosen to be 1 mm such that the code computationally generated only a monolayer of bubbles attached to the photoelectrode surface having a contact angle θ_c and projected surface area coverage f_A. The refractive and absorption indices of the photoelectrode were respectively taken as $n_p = 3.88$ and $k_p = 0.016$. The electrolyte and bubbles were non-absorbing with their respective refractive indices taken as $n_e = 1.33$ and $n_b = 1.0$. Figure S2(b) compares the area-averaged photoelectrode absorptance $\bar{A}$ predicted from our study with that reported in Ref.[4] for different projected surface area coverages f_A for bubble contact angle $\theta_c = 0^\circ$ or 90°. Here also, excellent agreement was observed, validating the accurate prediction of the effect of surface-attached bubbles on light transfer.

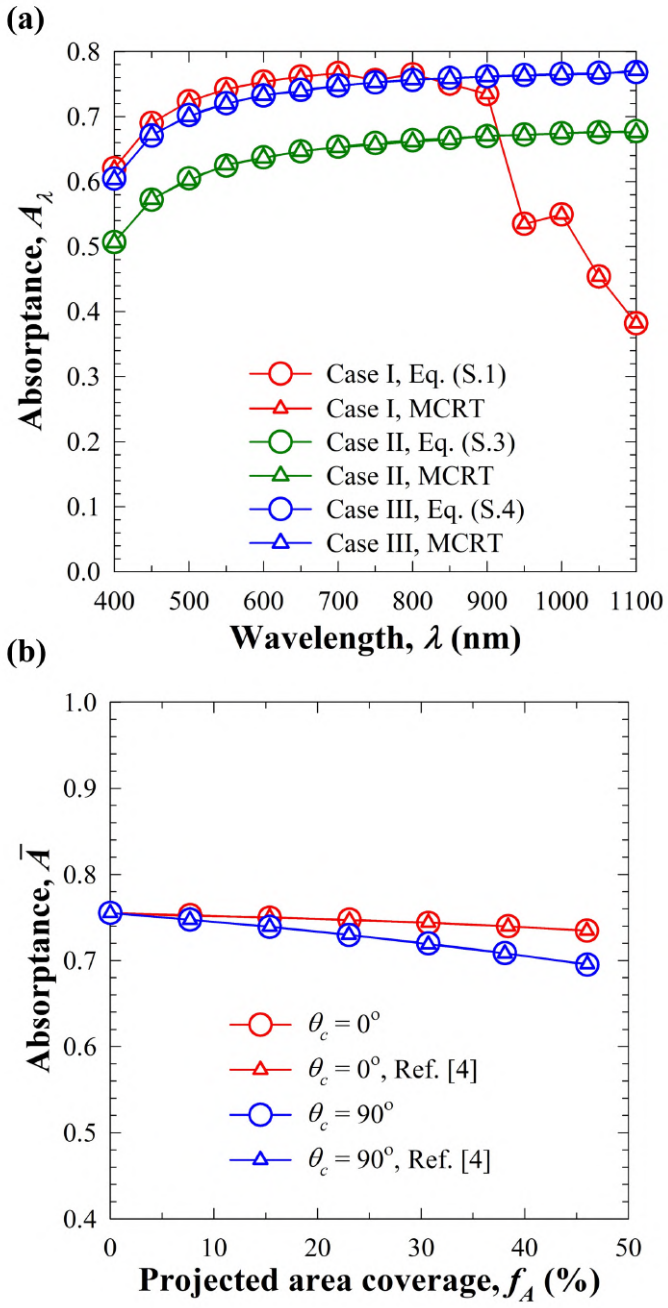

Figure S2: (a) Comparison of predicted area-averaged photoelectrode absorptance $\bar{A}_\lambda$ with the results from analytical expressions for Cases I, II, and III. (b) Comparison of predicted photoelectrode absorptance with the results reported in Ref.[4] for different projected surface area coverages f_A.

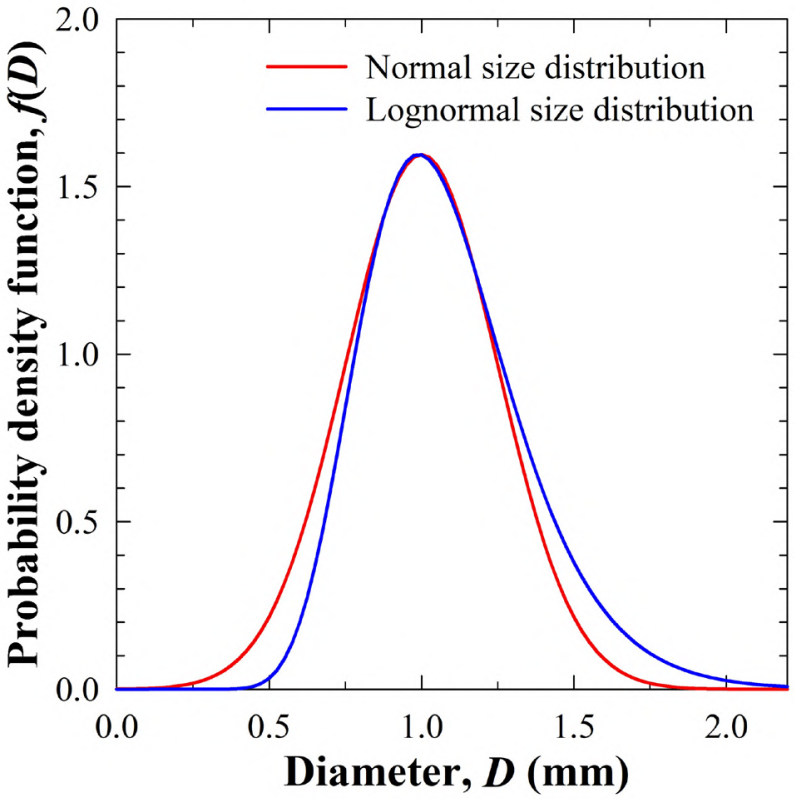

Figure S3: Comparison of probability density functions for polydisperse bubbles having either normal size distribution with mean diameter $\bar{D} = 1$ mm and standard deviation $\sigma = 0.25$ mm, or lognormal size distribution with mean $\mu = 0.05$ and standard deviation $\chi = 0.25$.

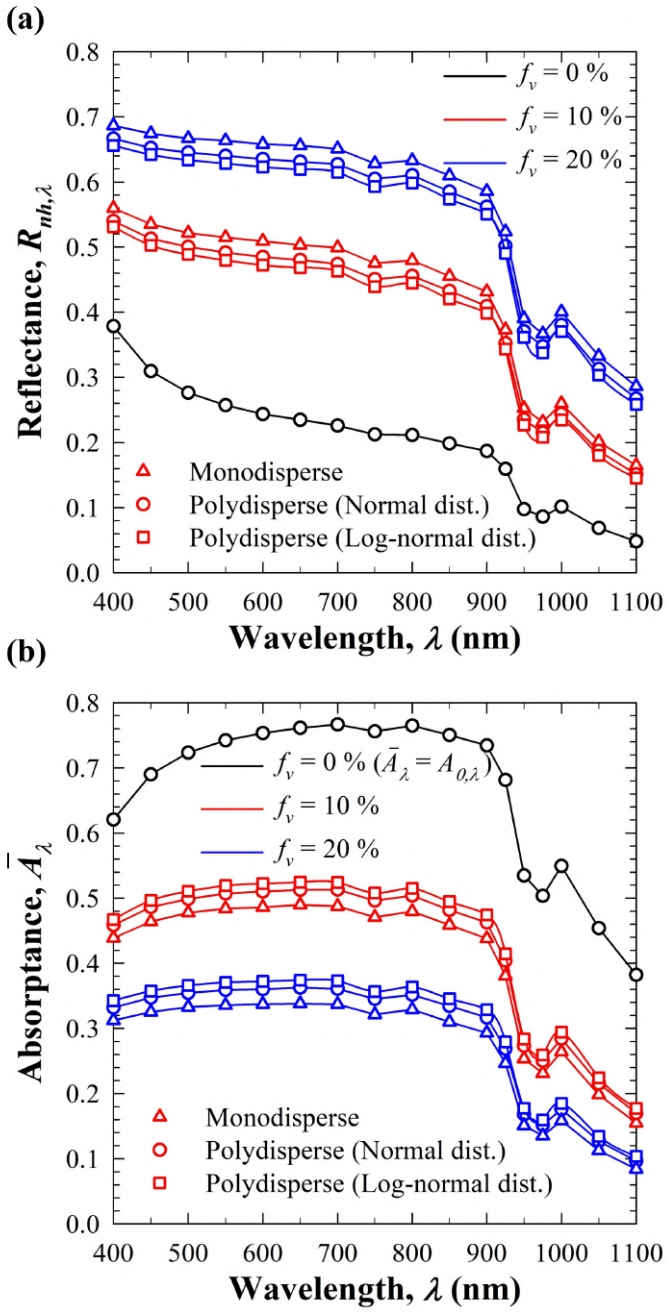

Figure S4: Comparison of (a) spectral normal-hemispherical reflectance $R_{nh,\lambda}$ and (b) spectral area-averaged photoelectrode absorptance $\bar{A}_\lambda$ for either monodisperse bubbles or polydisperse bubbles with normal or lognormal size distribution for mean bubble diameter of 300 µm and bubble volume fractions f_v of 10% or 20%.

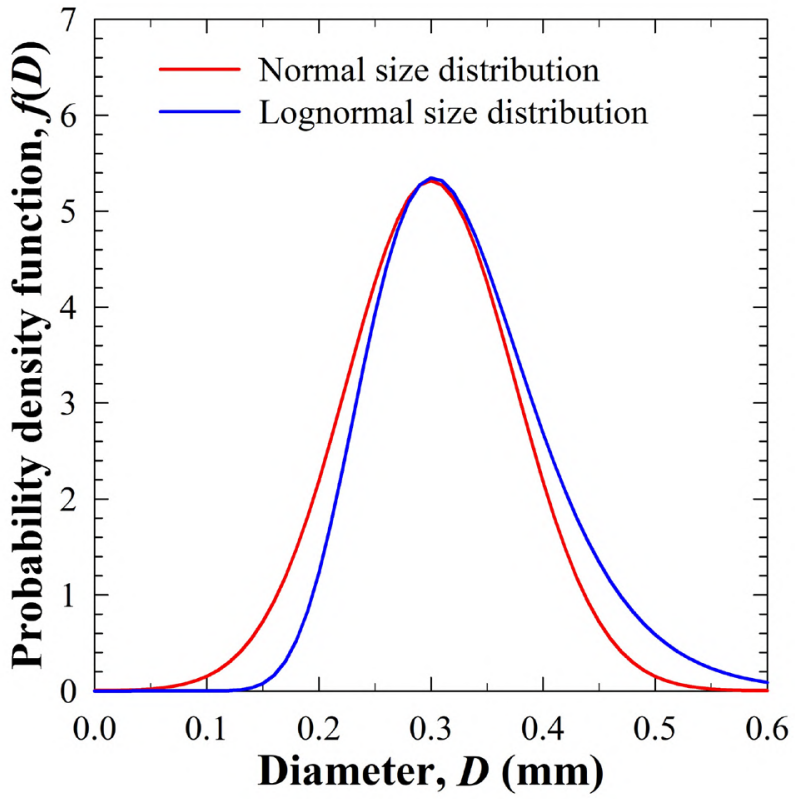

Figure S5: Comparison of probability density functions for polydisperse bubbles having either normal size distribution with mean diameter $\bar{D}$ = 300 µm and standard deviation σ = 75 µm, or lognormal size distribution with mean μ = -1.14 and standard deviation χ = 0.24.

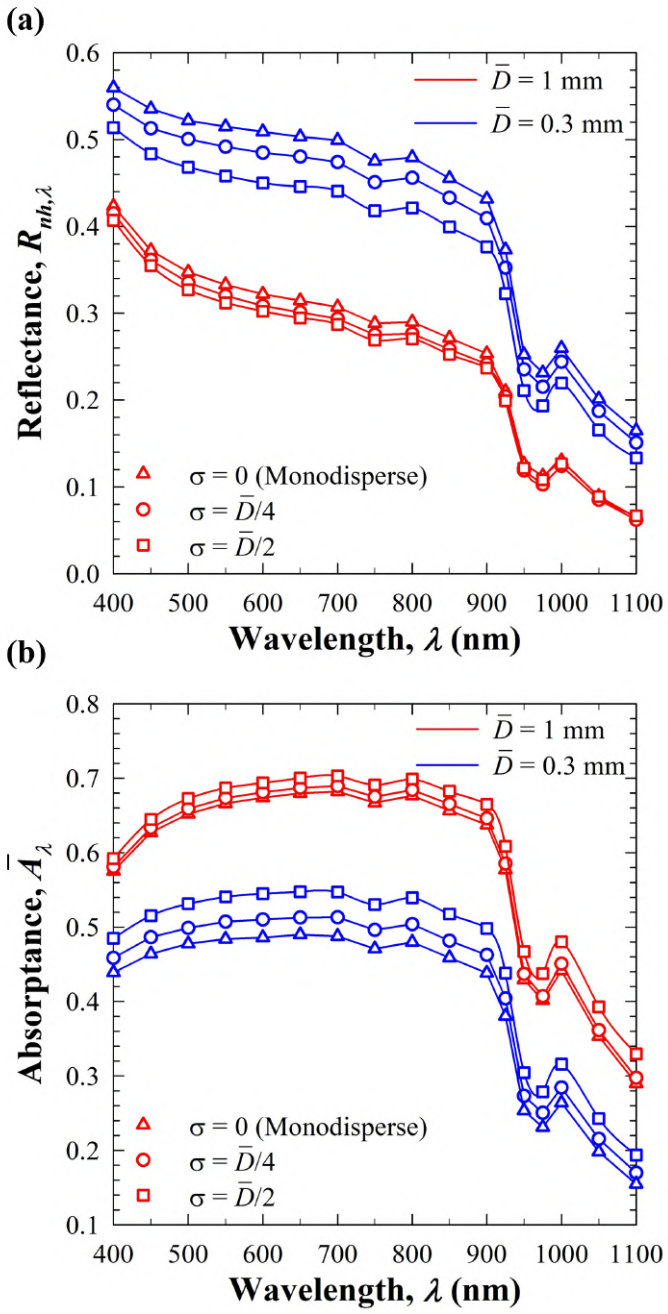

Figure S6: Comparison of (a) spectral normal-hemispherical reflectance $R_{nh,\lambda}$ and (b) spectral area-averaged photoelectrode absorptance $\bar{A}_\lambda$ for normally distributed polydisperse bubbles having mean bubble diameter $\bar{D} = 0.3$ or 1 mm and different standard deviations $\sigma = 0$, $\bar{D}/4$, or $\bar{D}/2$ for bubble volume fraction $f_v = 10\%$

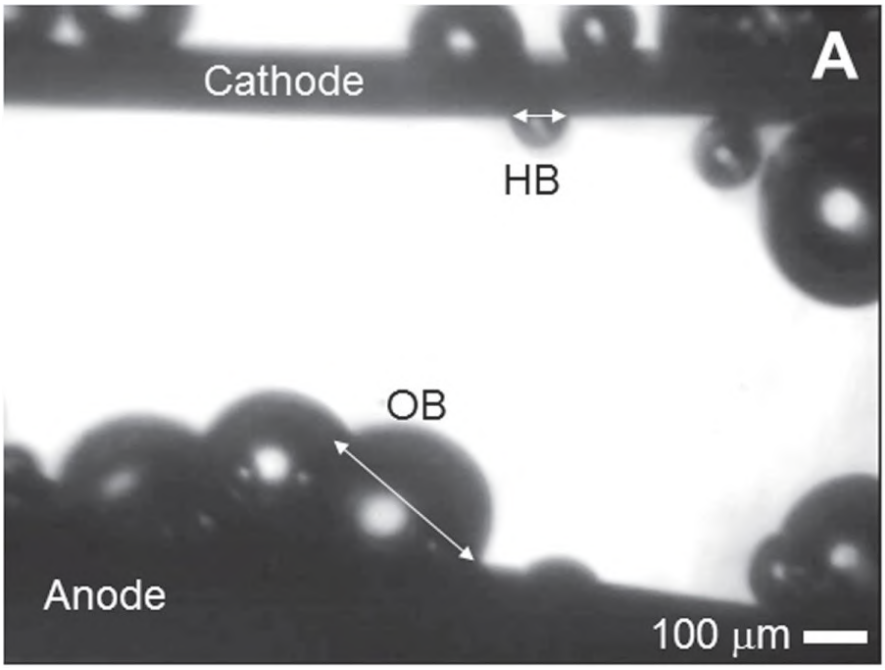

Figure S7: Comparison of the size of oxygen (OB) and hydrogen bubbles (HB) attached respectively to the cathode and anode during electrolysis of water. The bigger hydrogen bubble on the right end of cathode was a coalesced bubble (reprinted with permission from Ref. [5]. Copyright © 2016 The Japan Society of Mechanical Engineers)

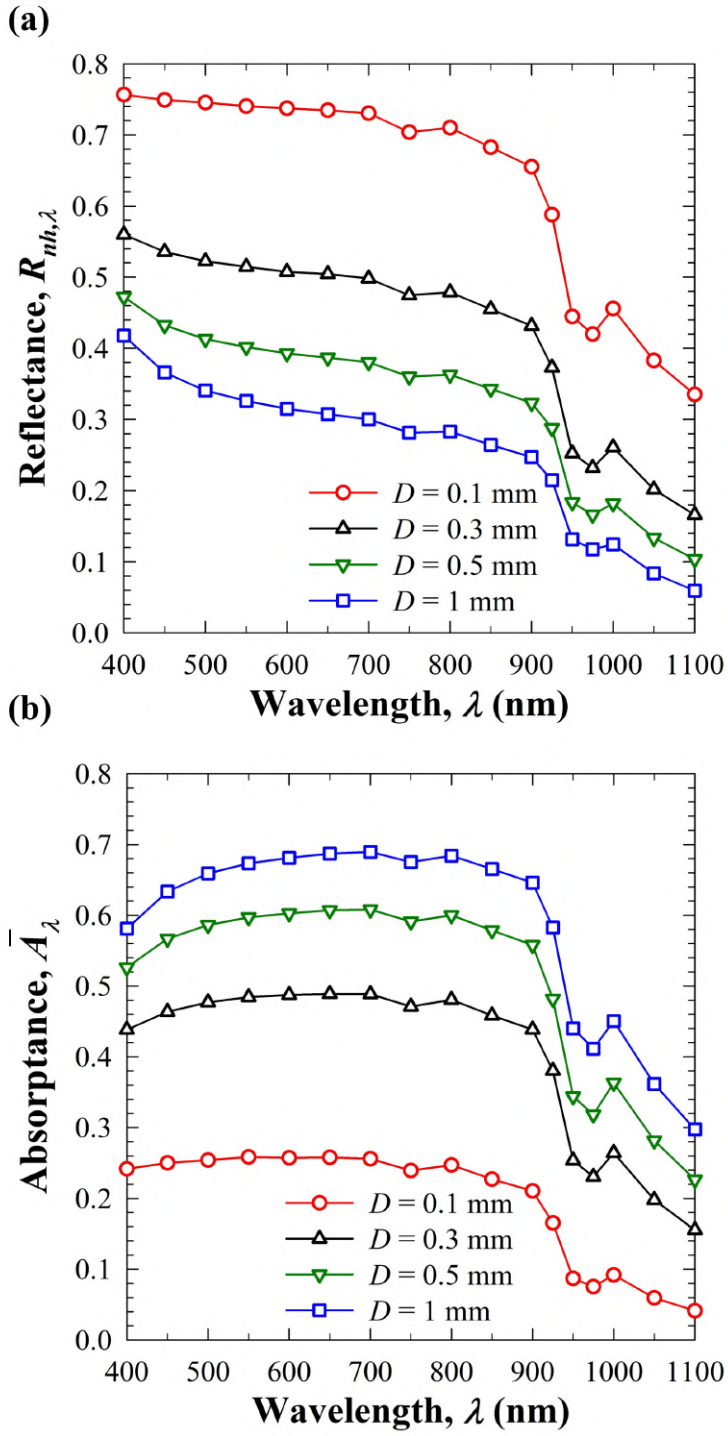

Figure S8: (a) Normal-hemispherical reflectance $R_{nh,\lambda}$ and (b) area-averaged photoelectrode absorptance $\bar{A}_\lambda$ as functions of wavelength λ for different bubble diameters D for bubble volume fraction $f_v = 10\%$ and bubble plume thickness $H = 10$ mm.

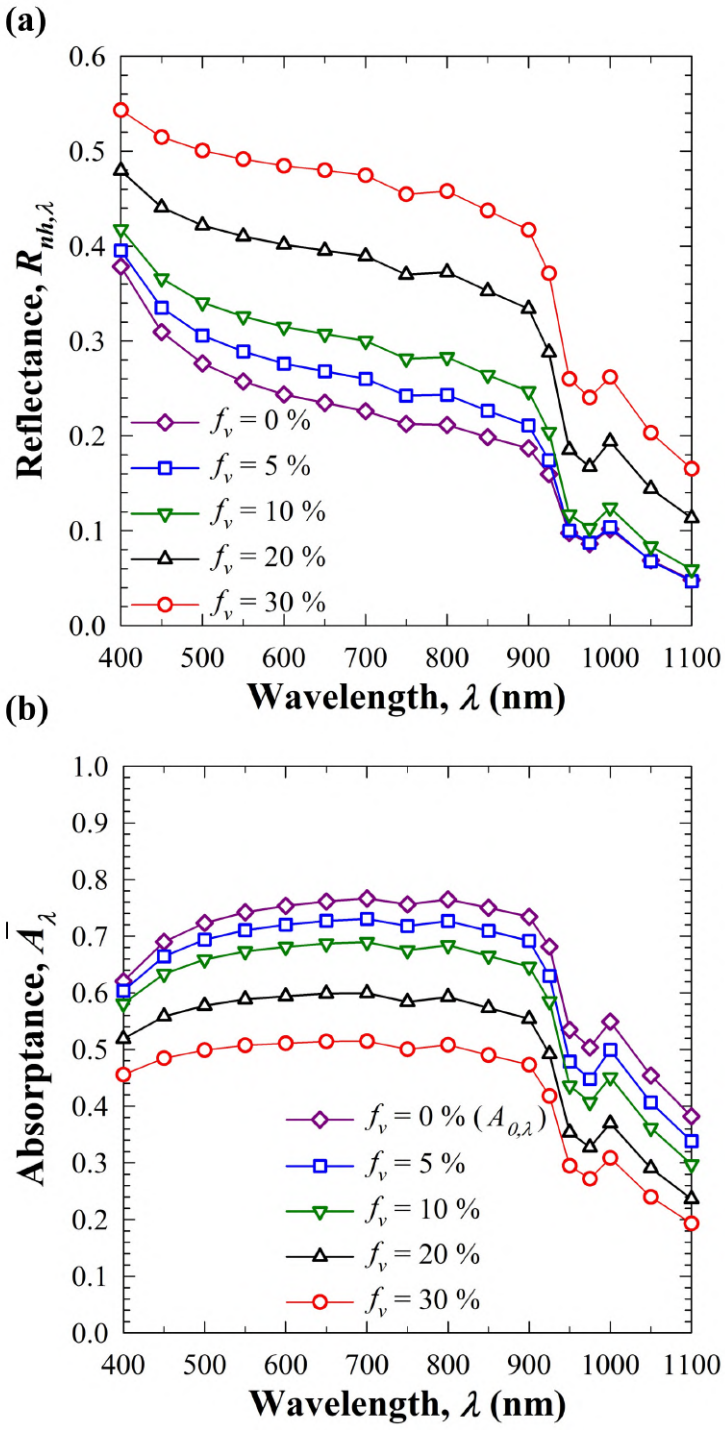

Figure S9: (a) Normal-hemispherical reflectance $R_{nh,\lambda}$ and (b) area-averaged photoelectrode absorptance $\bar{A}_\lambda$ as functions of wavelength λ for different bubble volume fractions f_v for bubble plume thickness $H = 10$ mm and bubble diameter $D = 1$ mm.

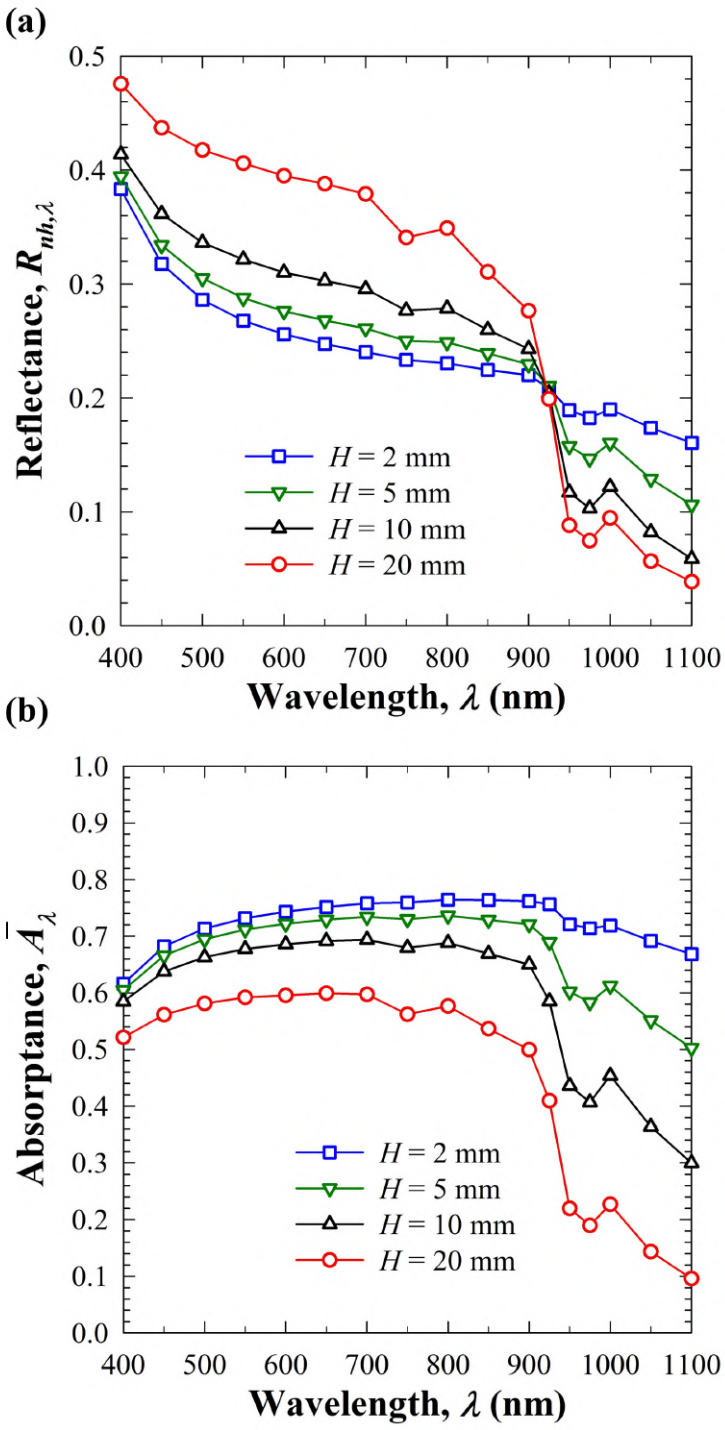

Figure S10: (a) Normal-hemispherical reflectance $R_{nh,\lambda}$ and (b) area-averaged photoelectrode absorptance $\bar{A}_\lambda$ as functions of wavelength λ for different bubble plume thicknesses H for bubble volume fraction $f_v = 10\%$ and bubble diameter $D = 1$ mm.

References

[1] K. Zhu, Y. Huang, J. Pruvost, J. Legrand, and L. Pilon, "Transmittance of transparent windows with non-absorbing cap-shaped droplets condensed on their backside," *Journal of Quantitative Spectroscopy and Radiative Transfer*, vol. 194, pp. 98–107, 2017.

[2] M. F. Modest and S. Mazumder, *Radiative Heat Transfer*. 4th ed., Academic Press, New York, NY, 2021.

[3] J. R. Howell, M. P. Mengüç, K. Daun, and R. Siegel, *Thermal Radiation Heat Transfer*. 7th ed., CRC Press, Boca Raton, FL, 2020.

[4] A. Bhanawat, K. Zhu, and L. Pilon, "How do bubbles affect light absorption in photoelectrodes for solar water splitting?," *Sustainable Energy & Fuels*, vol. 6, no. 3, pp. 910–924, 2022.

[5] K. Matsuura, Y. Yamanishi, C. Guan, and S. Yanase, "Control of hydrogen bubble plume during electrolysis of water," *Journal of Physics Communications*, vol. 3, no. 3, p. 035012, 2019.